glycoprotein. Indeed, there are numerous reports demonstrating the existence of anion transporters including OATs and Oatps (8, 30), although the direction of transport and specific location are not fully identified yet. Thus, we investigated the effect of anionic compounds on the brain penetration of COX inhibitors. So far, selective compounds for each anion transporter are not available. Thus, we selected probenecid due to the following two reasons: 1) it is a strong anion (31, 32), and 2) it can passively diffuse into tissues due to its lipophilicity. Thus, it would be expected that applying probenecid with COX inhibitors could estimate the function of both influx and efflux anion transporters at the BBB and/or BCSFB. Indeed, Galinsky et al. have demonstrated that probenecid can be used to evaluate the function of efflux anion transporters at the BBB in an in vivo animal model (33). Our data indicate that probenecid significantly increased K_p of both diclofenac and mefenamic acid. These results suggest that anion transporters might be involved in the transport of diclofenac and mefenamic acid. Moreover, considering the fact that the K_p of diclofenac and mefenamic acid was increased, rather than decreased, we suggest that probenecid may inhibit the efflux transporters at the BBB and/or BCSFB.

Thus, considering the finding that SLT-II increased brain penetration of these two COX inhibitors, it has been expected that SLT-II decreases the expressions /functions of efflux transporter for anionic compounds at the BBB and/or BCSFB. Recently, various efflux transporters are found on the BBB and BCSFB. Among them, Oatp2 and OAT3 have been reported as anion transporters (34 – 37). However, immunohistochemical studies have demonstrated that Oatp2 is located on the apical sides of the BBB, probably acting as an influx transporter (30). Thus, considering the results using probenecid, we investigated the expression of OAT3 in SLT-II-treated mice. Our results indicated that SLT-II significantly decreased the expression of OAT3. This suggests that the decreased expression of OAT3 might be one candidate efflux transporter to change brain penetration of COX inhibitors by SLT-II. In this study, we did not evaluate the impact of other anion transporters on the brain penetration of COX inhibitors. Thus, further work is required to fully understand this issue. Moreover, we must also determine which factors are important for regulating the BBB function after SLT-II treatment among the cytokines released by SLT-II or SLT-II itself since cytokines might regulate the function of transporters (7 – 9) and SLT-II increases the levels of cytokines including TNF-α and NOx in the plasma of rodents (11, 12, 38). However, the altered brain penetration of drugs was varied between the bacterial toxins since another bacterial toxin, endotoxin, did not alter K_p of either FD-4 or doxorubicin, even though endotoxin stimulated the release of cytokines (39).

In conclusion, SLT-II differentially affected the brain penetration of COX inhibitors. Among COX inhibitors investigated, SLT-II might preferentially alter brain penetration of diclofenac and mefenamic acid, rather than acetaminophen. Thus, considerable attention would be necessary when using COX inhibitors in patients with *E. coli* O157 infection. Moreover, one of the candidate transporters that may contribute to the change in brain penetration of COX inhibitors, OAT3, was evaluated. Together, these results caution us that bacterial and virus infections such as *E. coli* O157 (10, 11) and influenza virus (4, 5) might increase the risk of CNS side-effects of drugs transported by OAT3 and other efflux transporters.

Acknowledgment

This work was supported by a grant-in-aid from the Ministry of Health and Welfare, Japan to T.M. Preliminary data were presented at the Annual Meeting of the Pharmaceutical Society of Japan, Nagasaki, Japan, 2003.

References

1 Waldman RJ, Hall WN, McGee H, Van Amburg G. Aspirin as a risk factor in Reye's syndrome. JAMA. 1982;247:3089–3094.
2 Kasai T, Togashi T, Morishima T. Encephalopathy associated with influenza epidemics. Lancet. 2000;355:1558–1559.
3 Morishima T, Togashi T, Yokota S, Okuno Y, Miyazaki C, Tashiro M, et al. Encephalitis and encephalopathy associated with an influenza epidemic in Japan. Clin Infect Dis. 2002; 35:512–517.
4 Ichiyama T, Isumi H, Ozawa H, Matsubara T, Morishima T, Furukawa S. Cerebrospinal fluid and serum levels of cytokines and soluble tumor necrosis factor receptor in influenza virus-associated encephalopathy. Scand J Infect Dis. 2003;35:59–61.
5 Kawada J, Kimura H, Ito Y, Hara S, Iriyama M, Yoshikawa T, et al. Systemic cytokine responses in patients with influenza-associated encephalopathy. J Infect Dis. 2003;188:690–698.
6 Kawashima H, Watanabe Y, Morishima T, Togashi T, Yamada N, Kashiwagi Y, et al. NOx (nitrite/nitrate) in cerebral spinal fluids obtained from patients with influenza-associated encephalopathy. Neuropediatrics. 2003;34:137–140.
7 Kang YS, Ohtsuki S, Takanaga H, Tomi M, Hosoya K, Terasaki T. Regulation of taurine transport at the blood-brain barrier by tumor necrosis factor-α, taurine and hypertonicity. J Neurochem. 2002;83:1188–1195.
8 Strazielle N, Khuth ST, Murat A, Chalon A, Giraudon P, Belin MF, et al. Pro-inflammatory cytokines modulate matrix metalloproteinase secretion and organic anion transport at the blood-cerebrospinal fluid barrier. J Neuropathol Exp Neurol. 2003;62:1254–1264.
9 Theron D, Barraud de Lagerie S, Tardivel S, Pelerin H, Demeuse

P, Mercier C, et al. Influence of tumor necrosis factor-alpha on the expression and function of P-glycoprotein in an immortalised rat brain capillary endothelial cell line, GPNT. Biochem Pharmacol. 2003;66:579–587.

10 Kita E, Yunou Y, Kurioka T, Harada H, Yoshikawa S, Mikasa K, et al. Pathogenic mechanism of mouse brain damage caused by oral infection with Shiga toxin-producing Escherichia coli O157:H7. Infect Immun. 2000;68:1207–1214.

11 Zhao YL, Du J, Kanazawa H, Cen XB, Takagi K, Kitaichi K, et al. Shiga-like toxin II modifies brain distribution of a P-glycoprotein substrate, doxorubicin, and P-glycoprotein expression in mice. Brain Res. 2002;956:246–253.

12 Zhao YL, Cen XB, Ito M, Yokoyama K, Takagi K, Kitaichi K, et al. Shiga-like toxin II derived from Escherichia coli O157:H7 modifies renal handling of levofloxacin in rats. Antimicrob Agents Chemother. 2002;46:1522–1528.

13 Sun H, Dai H, Shaik N, Elmquist WF. Drug efflux transporters in the CNS. Adv Drug Deliv Rev. 2003;55:83–105.

14 Graff CL, Pollack GM. Drug transport at the blood-brain barrier and the choroid plexus. Curr Drug Metab. 2004;5:95–108.

15 Lee W, Kim RB. Transporters and renal drug elimination. Annu Rev Pharmacol Toxicol. 2004;44:137–166.

16 Khamdang S, Takeda M, Noshiro R, Narikawa S, Enomoto A, Anzai N, et al. Interactions of human organic anion transporters and human organic cation transporters with nonsteroidal anti-inflammatory drugs. J Pharmacol Exp Ther. 2002;303:534–539.

17 Sweet DH, Miller DS, Pritchard JB, Fujiwara Y, Beier DR, Nigam SK. Impaired organic anion transport in kidney and choroid plexus of organic anion transporter 3 (Oat3 (Slc22a8)) knockout mice. J Biol Chem. 2002;277:26934–26943.

18 Kojima R, Sekine T, Kawachi M, Cha SH, Suzuki Y, Endou H. Immunolocalization of multispecific organic anion transporters, OAT1, OAT2, and OAT3, in rat kidney. J Am Soc Nephrol. 2002;13:848–857.

19 Choudhuri S, Cherrington NJ, Li N, Klaassen CD. Constitutive expression of various xenobiotic and endobiotic transporter mRNAs in the choroid plexus of rats. Drug Metab Dispos. 2003;31:1337–1345.

20 Masuda S, Saito H, Inui K. Interactions of nonsteroidal anti-inflammatory drugs with rat renal organic anion transporter, OAT-K1. J Pharmacol Exp Ther. 1997;283:1039–1042.

21 Morita N, Kusuhara H, Sekine T, Endou H, Sugiyama Y. Functional characterization of rat organic anion transporter 2 in LLC-PK1 cells. J Pharmacol Exp Ther. 2001;298:1179–1184.

22 Sugiyama D, Kusuhara H, Taniguchi H, Ishikawa S, Nozaki Y, Aburatani H, et al. Functional characterization of rat brain-specific organic anion transporter (Oatp14) at the blood-brain barrier: high affinity transporter for thyroxine. J Biol Chem. 2003;278:43489–43495.

23 Shitara Y, Sugiyama D, Kusuhara H, Kato Y, Abe T, Meier PJ, et al. Comparative inhibitory effects of different compounds on rat oatpl (slc21a1)- and Oatp2 (Slc21a5)-mediated transport. Pharm Res. 2002;19:147–153.

24 Emoto A, Ushigome F, Koyabu N, Kajiya H, Okabe K, Satoh S, et al. H(+)-linked transport of salicylic acid, an NSAID, in the human trophoblast cell line BeWo. Am J Physiol Cell Physiol. 2002;282:1064–1075.

25 Santamaria A, Rios C, Solis-Hernandez F, Ordaz-Moreno J, Gonzalez-Reynoso L, Altagracia M, et al. Systemic DL-kynurenine and probenecid pretreatment attenuates quinolinic acid-induced neurotoxicity in rats. Neuropharmacology. 1996; 35:23–28.

26 Cox DS, Scott KR, Gao H, Raje S, Eddington ND. Influence of multidrug resistance (MDR) proteins at the blood-brain barrier on the transport and brain distribution of enaminone anti-convulsants. J Pharm Sci. 2001;90:1540–1552.

27 Hirai T, Matsumoto S, Kishi I. Simultaneous analysis of several non-steroidal anti-inflammatory drugs in human urine by high-performance liquid chromatography with normal solid-phase extraction. J Chromatogr B Biomed Sci Appl. 1997;692:375–388.

28 Mikami E, Goto T, Ohno T, Matsumoto H, Inagaki K, Ishihara H, et al. Simultaneous analysis of anthranilic acid derivatives in pharmaceuticals and human urine by high-performance liquid chromatography with isocratic elution. J Chromatogr B Biomed Sci Appl. 2000;744:81–89.

29 Alkharfy KM, Frye RF. High-performance liquid chromatographic assay for acetaminophen glucuronide in human liver microsomes. J Chromatogr B Biomed Sci Appl. 2001;753:303–308.

30 Gao B, Stieger B, Noe B, Fritschy JM, Meier PJ. Localization of the organic anion transporting polypeptide 2 (Oatp2) in capillary endothelium and choroid plexus epithelium of rat brain. J Histochem Cytochem. 1999;47:1255–1264.

31 Ohtsuki S, Asaba H, Takanaga H, Deguchi T, Hosoya K, Otagiri M, et al. Role of blood-brain barrier organic anion transporter 3 (OAT3) in the efflux of indoxyl sulfate, a uremic toxin: its involvement in neurotransmitter metabolite clearance from the brain. J Neurochem. 2002;83:57–66.

32 Sugiyama D, Kusuhara H, Shitara Y, Abe T, Meier PJ, Sekine T, et al. Characterization of the efflux transport of 17beta-estradiol-D-17beta-glucuronide from the brain across the blood-brain barrier. J Pharmacol Exp Ther. 2001;298:316–322.

33 Galinsky RE, Flaharty KK, Hoesterey BL, Anderson BD. Probenecid enhances central nervous system uptake of 2',3'-dideoxyinosine by inhibiting cerebrospinal fluid efflux. J Pharmacol Exp Ther. 1991;257:972–978.

34 Kikuchi R, Kusuhara H, Sugiyama D, Sugiyama Y. Contribution of organic anion transporter 3 (Slc22a8) to the elimination of p-aminohippuric acid and benzylpenicillin across the blood-brain barrier. J Pharmacol Exp Ther. 2003;306:51–58.

35 Nagata Y, Kusuhara H, Endou H, Sugiyama Y. Expression and functional characterization of rat organic anion transporter 3 (rOat3) in the choroid plexus. Mol Pharmacol. 2002;61:982–988.

36 Hosoya K, Ohtsuki S, Terasaki T. Recent advances in the brain-to-blood efflux transport across the blood-brain barrier. Int J Pharm. 2002;248:15–29.

37 Kusuhara H, Sekine T, Utsunomiya-Tate N, Tsuda M, Kojima R, Cha SH, et al. Molecular cloning and characterization of a new multispecific organic anion transporter from rat brain. J Biol Chem. 1999;274:13675–13680.

38 Kitaichi K, Nakayama H, Ueyama J, Nadai M, Baba K, Takagi K, et al. Down-regulation of cytochrome P450 proteins and its activities by Shiga-like toxin II from Escherichia coli O157:H7. Biochem Pharmacol. 2004; 67:1427–1435.

39 Zhao YL, Du J, Kanazawa H, Sugawara A, Takagi K, Kitaichi K, et al. Effect of endotoxin on doxorubicin transport across blood-brain barrier and P-glycoprotein function in mice. Eur J Pharmacol. 2002;445:115–123.

Increased neuronal expression of alpha B-crystallin in the human olivary hypertrophy

Kazuko Fukushima[1], Yuji Mizuno[1], Masamitsu Takatama[2] and Koichi Okamoto[1]

[1]Department of Neurology, Gunma University Graduate School of Medicine, Maebashi, Gunma 371-8511, Japan and [2]Department of Internal Medicine, Geriatrics Research Institute and Hospital, Maebashi, Gunma 371-0847, Japan

Correspondence to: Koichi Okamoto, Department of Neurology, Gunma University Graduate School of Medicine, 3-39-22, Showa-machi, Maebashi, Gunma 371-8511, Japan
Phone: + 81-27-220-8060
Fax: +81-27-220-8067
E-mail: okamotok@med.gunma-u.ac.jp

Abstract

We studied morphologic changes in olivary hypertrophy from dentato-olivary tract lesions by immunohistologic methods with anti-alpha B-crystallin and anti-heat shock protein 27 (HSP 27). The majority of central chromatolysis-like enlarged neurons, which are frequently seen in the early stages of olivary hypertrophy on ipsilateral lesions, showed a marked expression of alpha B-crystallin; however, HSP 27 did not show increased expression in those neurons. In the later stages of olivary hypertrophy, increased expressions of alpha B-crystallin varied in the remaining neurons and the expression of HSP 27 increased in hypertrophied astrocytes, although the expression of alpha B-crystallin in hypertrophic astrocytes was not prominent. The accumulation of alpha B-crystallin and HSP 27 may represent responses to pathologic conditions.

Keywords: olivary hypertrophy, heat shock protein, alpha B-crystallin;, immunohistochemistry, inferior olive

Introduction

Olivary hypertrophy or pseudohypertrophy has been shown to result from lesions of dentato-rubro-olivary triangles, particularly from ipsilateral central tegmental tract lesions [1-5]. It has therefore been accepted that an anterograde transneuronal (transsynaptic) mechanism is involved in the pathogenesis of olivary hypertrophy. Our group previously suggested that fundamental changes in the neurons in olivary hypertrophy occur in the rough endoplasmic reticulum [6], and also described that the Golgi apparatus is frequently affected in degenerating neurons in the inferior orivary nucleus from the early stages after central tegmental tract lesions [7]. The Golgi apparatus is also affected in neurons of inferior olives in patients with multiple system atrophy [8].

Heat shock proteins (HSPs) or stress proteins play a role in normal central nervous system (CNS) development and function, and are enhanced after traumatic injury to the brain and during neurodegenerative diseases [9-14]. HSPs are classified according to their molecular weight, and the 27, 60 and 70kDa families have been mostly studied. Alpha B-crystallin is a member of the HSP family, is stress-inducible and has chaperone-like properties, preventing the aggregation of denatured proteins during times of cell stress. In the normal CNS, low-level alpha B-crystallin is found in astrocytes and oligodendrocytes, but not in neurons, showing increased expression in these glial cells in various neuropathological conditions [15].

Alpha B-crystallin is also expressed in ballooned neurons and in neurons in several pathologic conditions [4, 15, 16]. We observed an increased expression of alpha B-crystallin in the majority of neurons in the inferior orivary nucleus from the early stages after central tegmental tract lesions. We also examined HSP 27 in human olivary

hypertrophy by immunohistochemical analysis.

Methods

The brains of 6 autopsied patients with lesions in the dantato-olivary pathway after survival periods from 6 days to 15 months were available [6,7]. A short summary of the clinicopathologic findings in patients with dentato-olivary pathway lesions is shown in Table 1. Brains from 5 patients without pathologic changes served as controls. The brains were fixed with 4% paraformaldehyde in phosphate-buffered solution (pH7.4), and then embedded in paraffin; 5 μm-thick serial transverse sections of the medullas were stained with hematoxylin-eosin and Klüver-Barrera.

Immunohistochemistry was also carried out with the following antibodies: anti-human alpha B-crystallin (polyclonal, Novo Castra, 1:20,000), anti-heart shock protein 27 (HSP 27) (monoclonal, Chemicon, 1:400), anti-phosphorylated neurofilament antibody SMI-31 (monoclonal, Sternberger, 1:5,000), anti-non-phosphorylated neurofilament antibody SMI-32 (monoclonal, Sternberger, 1:1,000), and anti-glial fibrillary acidic protein (GFAP) (polyclonal, Dakopatts, 1:10,000). The sections were blocked in a solution supplied with the Histofine SAB-PO kit (Nichirei) for 30 min at room temperature, labeled with the first antibody at 4°C overnight, washed in PBS for 30 min, incubated with the second antibody provided with the Histofine SAB-PO kit (Nichirei), washed in PBS for 30 min, and then visualized by the avidin-biotin-peroxidase method. The sections were weakly counterstained with hematoxylin.

Results

Many enlarged neurons, resembling central chromatolysis, were noted in the inferior olivary nuclei from the side ipsilateral to the pontine lesions in patients 1, 2 and 3 without astrocytic reactions (Fig. 1A). Neurons decreased in the later stages of deafferentation (patients 4, 5 and 6), while the remainder was hypertrophied with frequent cytoplasmic vacuoles, and large gemistocytic astrocytes were also prominent at these stages.

In the medullas of 5 control brains, alpha B-crystallin was expressed in astrocytes and oligodendrocytes, and was not expressed in the neurons of inferior olivary nuclei. In patients 1, 2 and 3 shown in Table 1, the majority of central chromatolysis-like enlarged neurons, which are frequently seen in the early stages of olivary hypertrophy, showed a marked expression of alpha B-crystallin in the cytoplasm and their proximal processes on ipsilateral lesions (Fig. 1B); however neurons in the contralateral inferior olive did not show increased alpha B-crystallin expression (Fig. 1C). Scattered astrocytes and oligodendrocytes also expressed alpha B-crystallin as controls (Figs. 1B, 1C). In patients 4, 5 and 6, alpha B-crystallin immunoreactivity varied, namely the remaining neurons in the inferior olivary nuclei were weakly to strongly immunostained (Fig. 2A), but in contrast, increased alpha B-crystallin immunoreactivity was not prominent in the majority of hypertrophied astrocytes (Fig.

2A) which were strongly immunostained with GFAP (Fig. 2B). HSP 27 did not show increased expression in the neurons in all examined medullas. In the later stages of olivary hypertrophy, HSP 27 was strongly immunostained in hypertrophied astrocytes but not in enlarged neurons (Fig. 2C). Neurofilamentous hyperplasia was seen in the many remaining neurons in the chronic stages of olivary hypertrophy; however, SMI-31-positive phosphorylated neurofilamentous hyperplasia was not observed in the examined inferior olivary neurons (data not shown).

Discussion

In general, transneuronal (transsynaptic) degeneration caused by the loss of input by afferent neurons during adulthood is characterized by the atrophy of targeted neurons with mild glial reaction [17, 18]. The variable effects of afferent disconnection relate not only to age but also to a specific nuclear group. Synaptophysin immunostaining showed that presynaptic terminals in the inferior olivary nucleus changed their distribution during the course of olivary hypertrophy [4]. Transneuronal degeneration in the human inferior orivary nuclei showed a unique pathologic reaction, characterized by neuronal enlargement and marked astrocytic reactions [1, 3, 5]. Our group previously reported that central chromatolysis-like enlarged neurons in the inferior olivary nuclei were already and frequently present 6 days after pontine hemorrhages: an electron microscopic study revealed round, electron-dense granules in the rough endoplasmic reticulum of the enlarged neurons, suggesting that secretory processes are impaired in neurons of the olivary hypertrophy [6]; Barron et al. [19] reported similar fine structures. Our group also reported that the Golgi apparatus of enlarged neurons in inferior olivary nuclei in the early stages after central tegmental tract lesions lost its network-like configuration, and was reduced to numerous small disconnected granules (fragmentation) [7]. The results suggest that the Golgi apparatus is also affected in degenerating neurons by an anterograde transneuronal mechanism.

In this study, we described that the majority of central chromatolysis-like enlarged neurons, which are frequently seen in the early stages of olivary hypertrophy, showed an increased expression of alpha B-crystallin, although HSP 27 was not expressed in the neurons. In the later stages of olivary hypertrophy, the increased expression of alpha B-crystallin was variable in the remaining neurons, but in contrast, the expression of alpha B-crystallin was not prominent in hypertrophied astrocytes, although HSP 27 showed increased expression in those astrocytes. Several studies have demonstrated that alpha B-crystallin has a cytoprotective function under various stress conditions [9, 10, 15]. Iwaki et al. [15] reported that some neurons in several neurodegenerative disorders were also immnunolabeled with anti-alpha B-crystallin antiserum. Ogawa et al. [20] examined 9 cases of inferior olivary pseudohypertrophy by immunohistochemical methods and found alpha B-crystallin-positive neurons in all cases. The number of alpha B-crystallin-positive neurons was variable: two cases were rare and seven cases were occasional to frequent. Their number was relatively

correlated with the degree of both neuronal loss and gliosis, and it was considered that this variability may be associated with age and lesion location, and that alpha B-crystallin might play a protective role as a molecular chaperone in olivary pseudohypertrophy. Unfortunately, they did not examine the early stages of orivary hypertrophy. In our study, alpha B-crystallin immunoreactivity in almost all enlarged neurons increased from the early stages of olivary hypertrophy.

Kato et al. [21] did a comparative study on the expression of alpha B-crystallin and HSP 27 by ballooned neurons in several neurodegenerative diseases. Despite strong homology in the amino acid sequence between alpha B-crystallin and HSP 27, the proportion of positively stained ballooned neurons of Pick's disease and Creutzfeld-Jakob disease was lower with HSP 27 than with alpha B-crystallin, and the observations suggested that both reagents recognize different epitopes shared by some abnormal neurons in the examined diseases. In olivary hypertrophy, there was also a discrepancy of neuronal immunostaining between alpha B-crystallin and HSP 27.

Alpha B-crystallin is known to be upregulated in response to a wide variety of pathologic conditions associated with increased cellular stress. Transneuronal degeneration may act as cellular stress on neurons in the human inferior olivary nuclei. Ginsberg and Martin [22] showed that axonal bundle transection in the adult rat CNS induces two forms of remote degeneration in deaffentated target regions, transsynaptic neuronal atrophy, which is characterized by vacuolar neuronal degeneration, and apoptosis. Vacuolar degeneration has some similarities to the neuronal changes seen in olivary hypertrophy and to excitotoxic damage caused by the excessive activation of glutamate receptors in the hypothalamus and septum. Ginsberg et al. [23] suggested that postsynaptic glutamate receptor activation is a possible mechanism of transneuronal degeneration following CNS axtotomy. Transneuronal degeneration also occurred within the substantia nigra pars reticulata following injury to the striatum of adult rats and induced HSP 70 synthesis [18, 24]. Axotomied inferior olivary neurons undergo severe regressive modification leading to conspicuous cell loss, and the long-standing expression of several axon-growth-associated markers expressed in injured neurons revealed that they are endowed with strong intrinsic regeneration potential [17]. Contralateral cerebellotomy can induce olivary neuron hypertrophy in cats, indicating that the ratio of excitatory to inhibitory terminals is increased in hypertrophied neutrophils, whereas the monoaminergic input does not change [25]. Several mechanisms are proposed as mentioned above, however more studies are needed to clarify the precise morphogenesis of olivary hypertrophy due to transneuronal degeneration.

In this study, dissociation between GFAP and alpha B-crystallin immunoreactivity was present in hypertrophied astrocytes in the later stages, and similar dissociation has already been recognized in pathologic conditions [15, 26]. Alpha B-crystallin and GFAP may be regulated independently in astrocytes in different pathologic states.

In conclusion, this is the first report to observe increased alpha B-crystallin expression in the majority of degenerating neurons from the early stages of olivary hypertrophy, and the accumulation of alpha B-crystallin and HSP 27 may represent the responses to pathologic conditions.

Acknowledgments

This work was supported by a grant from the Ministry of Health, Labour and Welfare of Japan to K. Okamoto.

References

1. Goto N, Kaneko M. Olivary enlargement: Chronological and morphometric analyses. Acta Neuropathol (Berl) 1981; **54**: 275-282.

2. Horoupian DS, Wisniwski H. Neurofilamentous hyperplasia in inferior olivary hypertrophy. J Neuropathol Exp Neurol 1971; **30**: 571-582.

3. Jellinger K. Hypertrophy of the inferior olives. Report on 29 cases. Z Neurol 1973; **205**: 153-174.

4. Kawakami T, Kato T, Llena JF, Hirano A, Sasaki H. Altered synaptophysin-immunoreactive pattern in human olivary hypertrophy. Neurosci Lett 1994; **176**: 178-180.

5. Sohn D, Levine S. (1971) Hypertrophy of the olives: A report on 43 cases. In: Zimmerman HM (ed) *Progressive Neuropathology*, Vol 1, Grune and Stratton, NY, 1971; 202-217.

6. Okamoto K, Hirai S, Iizuka T, Watanabe M. Fundamental morphological changes in human olivary hypertrophy. Acta Pathol Jpn 1992; **42**: 408-413.

7. Takamine K, Okamoto K, Fujita Y, Sakurai A, Takatama M, Gonatas NK. The involvement of the neuronal Golgi apparatus and trans-Golgi network in the human olivary hypertrophy. J Neurol Sci 2000; **182**: 45-50.

8. Sakurai A, Okamoto K, Yaguchi M, Fujita Y, Mizuno Y, Nakazato Y, Gonatas NK. Pathology of the inferior olivary nucleus in patients with multiple system atrophy. Acta Neuropathol 2002; **103**: 550-554.

9. Che Y, Piao CS, Ham P-L, Lee J-K. Delayed induction of αB-crystallin, in activated glia cells of hippocampus in kainic acid-treated mouse brain. J Neurosci Res 2001; **65**: 425-431

10. Dabir DV, Trojanowski JQ, Richter-Landsberg C, Lee VM-Y, Forman MS. Expression of the small heat-shock protein αB-crustallin in tauopathies with glial pathology. Am J Pathol 2004; **164**: 155-166.

11. Head MW, Goldman JE (2000) Small heat shock proteins, the cytoskeleton, and inclusion body formation. Neuropathol Appl Neurobiol 2000; **26**: 304-312.

12. Minami M, Mizutani T, Kawanishi R, Suzuki Y, Mori H. Neuronal expression of αB

crystallin in cerebral infarction. Acta Neuropathol 2003; **105**: 549-554.

13. Ohtsuka K, Suzuki T. Roles of molecular chaperones in the nervous system. Brain Res Bull 2000; **53**: 141-146.

14. Schultz C, Dick Jr EJ, Cox AN, Hubbard GB, Braak E, Braak H. Expression of stress proteins alpha B-crystallin, ubiquitin, and hsp 27 in pallido-nigral spheroids of aged rhesus monkeys. Neurobiol Aging 2001; **22**: 677-682.

15. Iwaki T, Wisniewski T, Iwaki A, Corbin E, Tomokane N, Tateishi J, Goldman JE. Accumulation of αB-crystallin in central nervous system glia and neurons in pathologic conditions. Am J Pathol 1992; **140**: 345-356.

16. Yaguchi M, Nagashima K, Izumi T, Okamoto K. Neuropathological study of C57BL/6 Akita mouse, type 2 diabetic model: Enhanced expression of αB-crystallin in oligodendrocytes. Neuropathology 2003; **23**: 44-50.

17. Buffo A, Fronte M, Oestreicher AB, Rossi F. Degenerative phenomena and reactive modifications of the adult rat inferior olivary neurons following axotomy and disconnection from their targets. Neuroscience 1998; **85**: 587-604.

18. Stefanis L, Burke RE. Transneuronal degeneration in substantia nigra pars reticulata following striatal excitotoxic injury in adult rat: time-course, distribution and morphology of cell death. Neuroscience 1996; **74**: 997-1008.

19. Barron KD, Dentinger MP, Koeppen AH. Fine structure of neurons of the hypertrophied human inferior olive. J Neuropathol Exp Neurol 1982; **41**: 186-203.

20. Ogawa K, Uehara K, Minami M, Suzuki Y, Mizutani T. The pathological study for pseudohypertrophy of inferior olives. Proceedings in The 46th Annual Meetings of the Japanese Society of Neuropathology. Neuropathology 2005; **25**(2): A13 (abstract)

21. Kato S, Hirano A, Umahara T, Kato M, Herz F, Ohama E. Comparative immunohistochemical study on the expression of αB crystallin, ubiquitin and stress-response protein 27 in ballooned neurons in various disorders. Neuropathol Appl Neurobiol 1992; **18**: 335-340.

22. Ginsberg SD, Martin LJ. Axonal transection in adult rat brain induces transsynaptic apoptosis and persistent atrophy of target neurons. J Neurotraum 2002; **19**: 99-109.

23. Ginsberg SD, Portera-Cailliau C, Martin LJ. Fimbria-fornix transection and

excitotoxicity produce similar neurodegeneration in the septum. Neuroscience 1998; **88**: 1059-1071.

24. Yamada K, Goto S, Ushio Y. Occurrence of heat shock response in deafferented neurons in the substantia nigra of rats. Neuroscience 1994; **62**: 793-801.

25. De Zeeuw CI, Ruigrok TJH, Schalekamp MPA, Boesten AJP, Voogd J. Ultrastructural study of the cat hypertrophic inferior olive following anterograde tracing, immunohistochemsitry, and intracellular labeling. Eur J Morphol 1990; **28**: 240-255.

26. Imura T, Shimohama S, Sato M, Nishikawa H, Madono K, Akaike A, Kimura J. Differential expression of small heat shock proteins in reactive astrocytes after focal ischemia: possible role of β-adrenergic receptor. J Neurosci 1999; **19**: 9768-9779.

Figure Legends

Fig. 1
Many chromatolysis-like enlarged neurons were already present in the inferior olive from the side ipsilateral to the pontine lesion in patient 2 (A: Klüver-Barrera staining). The majority of central chromatolysis-like enlarged neurons show marked expression of alpha B-crystallin in the cytoplasm and proximal processes on the ipsilateral lesion (B); however neurons in the contralateral inferior olive did not show increased alpha B-crystallin expression (C). Astrocytes show alpha B-crystallin expression in their cytoplasm (C). Bar = 50 μm.

Fig. 2
The remaining neurons in the inferior olivary nuclei are weakly (double arrows) to strongly (single arrows) immunostained for alpha B-crystallin in Patient 6, whereas increased alpha B-crystallin immunoreactivity is not prominent in the majority of hypertrophied astrocytes (A). Panel B is an adjacent section immunostained with anti-GFAP antibody, indicating that the remaining neurons were negative (single and double arrows), whereas the hypertrophied astrocytes were strongly immunostained for GFAP (B). In later stages of olivary hypertrophy, HSP 27 is strongly immunostained in hypertrophied astrocytes, but HSP 27 does not show increased expression in the remaining neurons in Patient 5 (C). Bar = 50 μm.

Table 1 Six autopsied patients with dentato-olivary tract lesions
Age at death (years); M, male; F, female; Duration, survival period after onset; -, not apparent; 1+, mild; 2+, moderate; 3+, marked

Patients	Age	Sex	Clinicopathological findings	Duration	alpha B-crsytallin in neurons	HSP 27 in neurons	alpha B-crystallin in astrocytes	HSP 27 in astrocytes
1	75	M	Pontine hemorrhage	6 dayas	3+	—	1+	—
2	72	M	Pontine hemorrhage	11 days	3+	—	1+	—
3	76	M	Brainstem infarct	11 days	3+	—	1+	—
4	77	M	Brainstem infarct	4 months	1+〜3+	—	1+	2+
5	61	F	Pontine hemorrhage	6 months	1+〜3+	—	1+	3+
6	68	M	Metastatic cancer to cerebellum	15 months	1+〜3+	—	1+	2+

Fig. 1

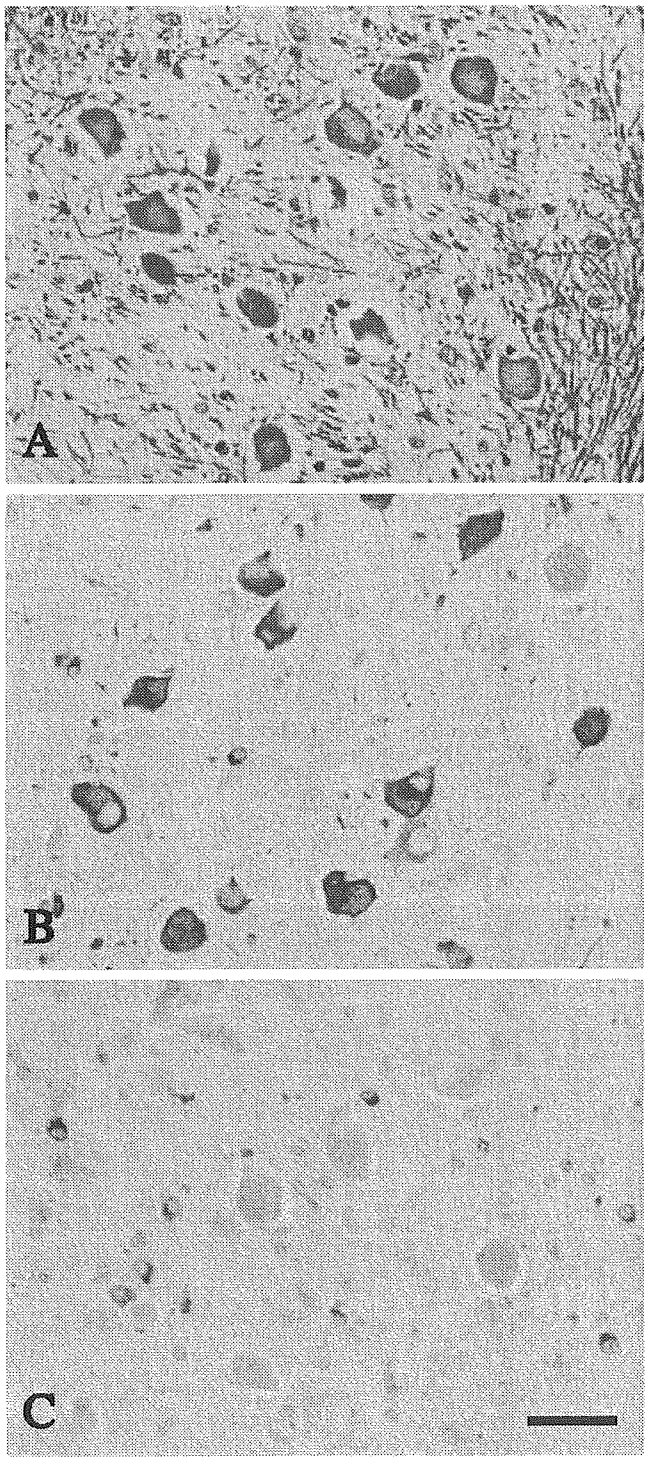

Fig. 2

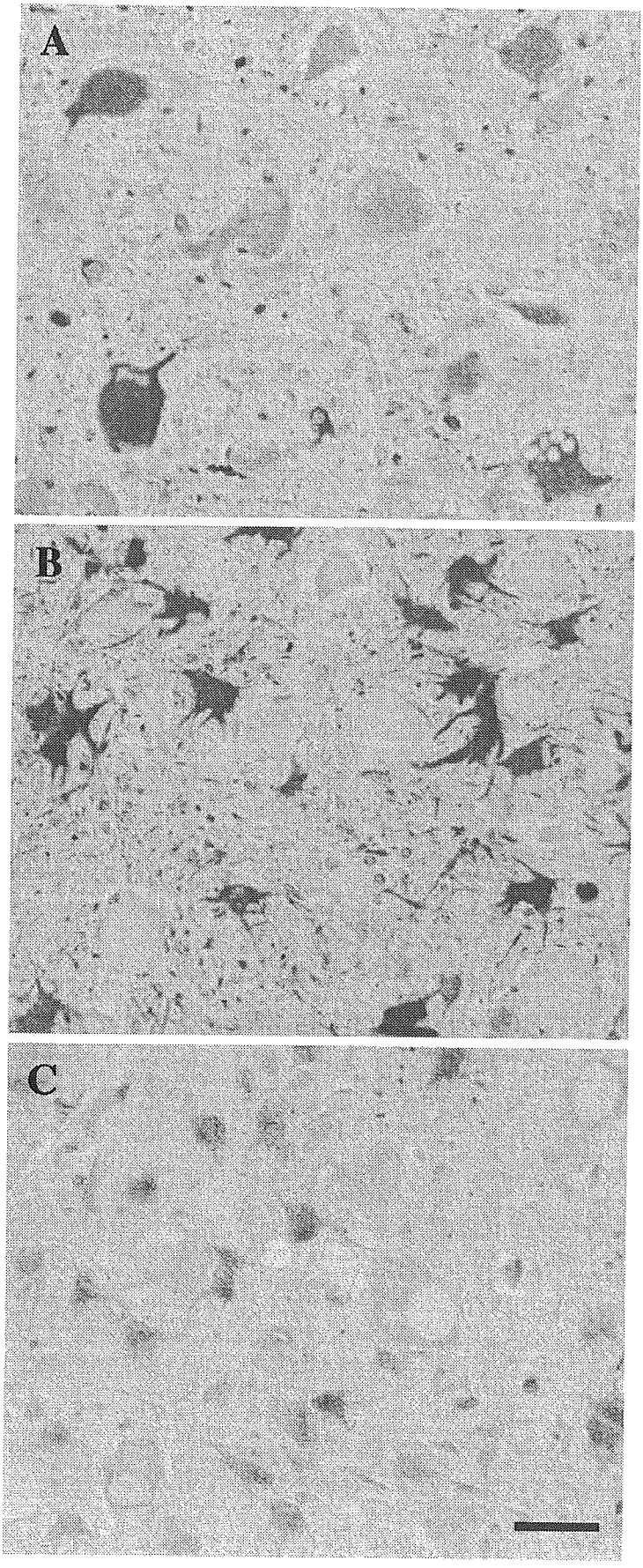

GH119
925.9
760.5
10%

Functional Anatomy of the Basal Ganglia in X-Linked Recessive Dystonia-Parkinsonism

Satoshi Goto, MD, PhD,[1] Lillian V. Lee, MD, MHA,[2] Edwin L. Munoz, MD,[3] Ikuo Tooyama, MD, PhD,[4] Gen Tamiya, PhD,[5] Satoshi Makino, PhD,[5] Satoshi Ando, PhD,[6] Marita B. Dantes, MD, MS,[2] Kazumichi Yamada, MD, PhD,[1] Sadayuki Matsumoto, MD, PhD,[6] Hideki Shimazu, MD, PhD,[7] Jun-ichi Kuratsu, MD, PhD,[1] Asao Hirano, MD, PhD,[8] and Ryuji Kaji, MD, PhD[7]

Dystonia is a neurological syndrome characterized by sustained muscle contractions that produce repetitive twisting movements or abnormal postures. X-linked recessive dystonia parkinsonism (XDP; DYT3; Lubag) is an adult-onset disorder that manifests severe and progressive dystonia with a high frequency of generalization. In search for the anatomical basis for dystonia, we performed postmortem analyses of the functional anatomy of the basal ganglia based on the striatal compartments (ie, the striosomes and the matrix compartment) in XDP. Here, we provide anatomopathological evidence that, in the XDP neostriatum, the matrix compartment is relatively spared in a unique fashion, whereas the striosomes are severely depleted. We also document that there is a differential loss of striatal neuron subclasses in XDP. In view of the three-pathway basal ganglia model, we postulate that the disproportionate involvement of neostriatal compartments and their efferent projections may underlie the manifestation of dystonia in patients with XDP. This study is the first to our knowledge to show specific basal ganglia pathology that could explain the genesis of dystonia in human heredodegenerative movement disorders, suggesting that dystonia may result from an imbalance in the activity between the striosomal and matrix-based pathways.

Ann Neurol 2005;58:7–17

Dystonia is defined as a syndrome of sustained muscle contraction frequently causing twisting or repetitive movements, or abnormal postures.[1] It is a common neurological disorder; however, the pathomechanism for the genesis of dystonia is poorly understood. X-linked recessive dystonia parkinsonism (XDP) was first described in 1976 by Lee and colleagues as endemic in Panay, Philippines.[2] It is a predominantly male, adult-onset disorder characterized by progressive and severe dystonia with a high frequency of generalization.[3–5] XDP is also named as DYT3 among 13 hereditary types of primary torsion dystonias designated DYT1 to DYT13.[6] Genetic analyses have assigned the disease locus DYT3 to Xq13.1.[7] In general, the dystonia in XDP dominates in the first 10 to 15 years of the illness and is associated with or replaced by parkinsonism in the later years of life.[4,5] Although the striatal lesion has long been thought to be the most striking pathology of XDP,[4,5,8–10] the functional anatomy of the basal ganglia in XDP remains unknown.

The mammalian striatum can be divided into two complementary and functionally distinct compartments, that is, the matrix and the striosomes, which are arranged in a mosaic pattern.[11,12] The matrix compartment forms the matrix-based pathways (ie, the direct and indirect pathways) that act as a push-pull system to increase or decrease movement. Until now, the focus in studies of the functional anatomy of basal ganglia disorders has centered on these two matrix-based pathways in efforts to explain the genesis of the disease-associated hyperkinetic or hypokinetic motor symptoms.[13,14] However, there also exists the third basal ganglia pathway, that is, the striosomal pathway, that originates in the striosomes and exerts critical motor control by modulating the nigral dopaminergic outputs.[15] The three-pathway basal ganglia model postulates that regulation

From the [1]Department of Neurosurgery, Graduate School of Medical Sciences, Kumamoto University, Kumamoto, Japan; [2]Child Neuroscience Department, Philippine Children's Medical Center, Quezon City, Philippines; [3]Pathology Division, Allied Medical Department, Philippine Children's Medical Center, Quezon City, Philippines, [4]Neurogene Unit, Molecular Neuroscience Research Center, Shiga University of Medical Science, Otsu, Japan; [5]Department of Molecular Life Science, Tokai University School of Medicine, Kanagawa, Japan; [6] Department of Neurology, Kitano Hospital and Neurological Center, Osaka, Japan; [7]Department of Neurology, Graduate School of Medicine, Tokushima University, Tokushima, Japan; and [8]Division of Neuropathology, Department of Pathology, Montefiore Medical Center, Bronx, NY.

Received Dec 27, 2004, and in revised form Mar 30, 2005. Accepted for publication Apr 8, 2005.

Published online May 23, 2005, in Wiley InterScience (www.interscience.wiley.com). DOI: 10.1002/ana.20513

Address correspondence to Dr Goto, Department of Neurosurgery, Graduate School of Medical Sciences, Kumamoto University, Kumamoto 860-8556, Japan.
E-mail: sgoto@kaiju.medic.kumamoto-u.ac.jp

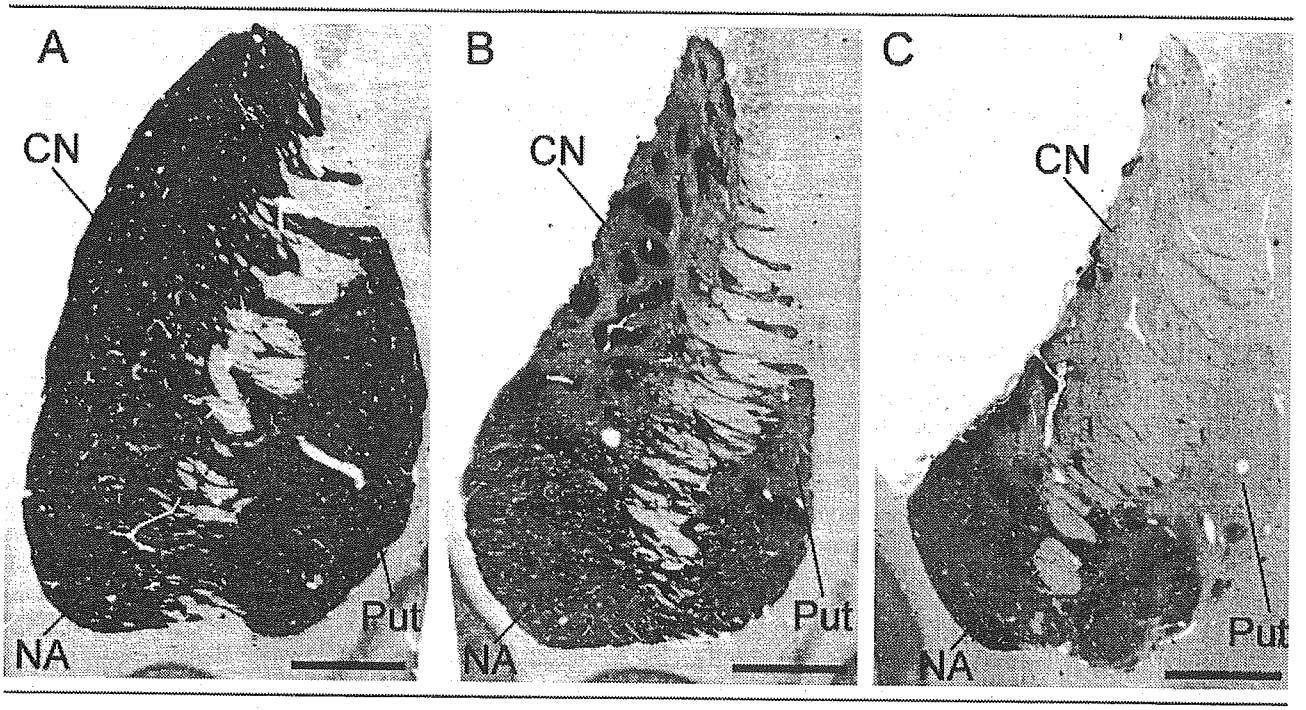

Fig 1. The striatum stained for calcineurin (CaN) in normal control and X-linked recessive dystonia parkinsonism (XDP) patients. (A) CaN staining of the striatum from a normal control. Strong CaN labeling is diffusely distributed in the entire striatum including the caudate nucleus (CN), putamen (Put), and nucleus accumbens (NA). (B, C) CaN staining of the striatum from patients with XDP. In XDP with dystonia (XDP-D) (B), two distinct compartments, that is, CaN^+ patches and interpatch area poor in CaN labeling, are found in the neostriatum. In XDP patients who had parkinsonism in the advanced stage (XDP-P) (C), CaN labeling is markedly diminished in the entire neostriatum, where CaN^+ patches are merely found. Scale bar (A–C) = 5mm.

of movement by the basal ganglia depends not only on the balance of activity between the matrix-based direct and indirect pathways, but also on the activity balance between these pathways and the striosomal pathway.[15] Here, we show that in the XDP neostriatum, the matrix compartment is relatively spared, whereas the striosomes are severely depleted. Our findings suggest that the differential involvement of striatal compartments that leads to an imbalance in the activity between the striosomal and matrix-based pathways may underlie the manifestation of dystonia in XDP.

Materials and Methods

Autopsied Materials and Tissue Preparation

Brain tissues obtained at autopsy from seven male Filipino XDP patients were examined. Their ages ranged from 42 to 59 years, and the disease duration ranged from 3 to 14 years. Among these patients, five manifested dystonia and the other two had parkinsonism in the advanced stage. Autopsied brains from seven age-matched neurologically normal controls were also examined. The tissues were fixed in 10% neutral formalin, sliced, and embedded in paraffin, and 6 μm sections were cut on a microtome and mounted onto MAS-coated glass slides (Matsunami Glass, Osaka, Japan). Conventional neuropathological examinations were performed using Nissl, Klüver–Barrera, and hematoxylin and eosin staining.

Immunohistochemistry

After routine deparaffinization, rehydration, and blocking of endogenous peroxidase activity, all sections to be used for immunostaining were processed for microwave-enhanced antigen retrieval.[16] Slide-mounted sections immersed in 0.01M sodium citrate buffer (pH 6.0) were placed for 15 minutes into a 700-W microwave oven at maximum power. Rabbit affinity-purified polyclonal antibody to calcineurin (CaN), previously characterized and used in other studies,[17–19] rabbit polyclonal antibody to calbindin (Calb; Chemicon International, Temecula, CA), rabbit polyclonal antibody to tyrosine hydroxylase (TH; Chemicon), rabbit polyclonal antibody to glial fibrillary acidic protein (GFAP; DAKO, Glostrup, Denmark), and rabbit polyclonal antibody to choline acetyltransferase (ChAT; Chemicon) were used as primary antibodies. The sections were blocked with 3% bovine serum albumin (BSA) in phosphate-buffered saline (PBS, pH 7.2) for 1 hour and then incubated overnight at room temperature in 3% BSA-PBS containing the primary antibodies. For the visualization of bound antibodies, we used the Elite ABC Kit (Vector, Burlingame, CA). Diaminobenzidine (DAB) was used as chromogen. Some sections were further processed for the enhancement of DAB reaction products.[20] Serially adjacent midbrain sections stained for TH and CaN were pretreated with $KMnO_4$ and oxalic acid to bleach the melanin pigmentation.[21]

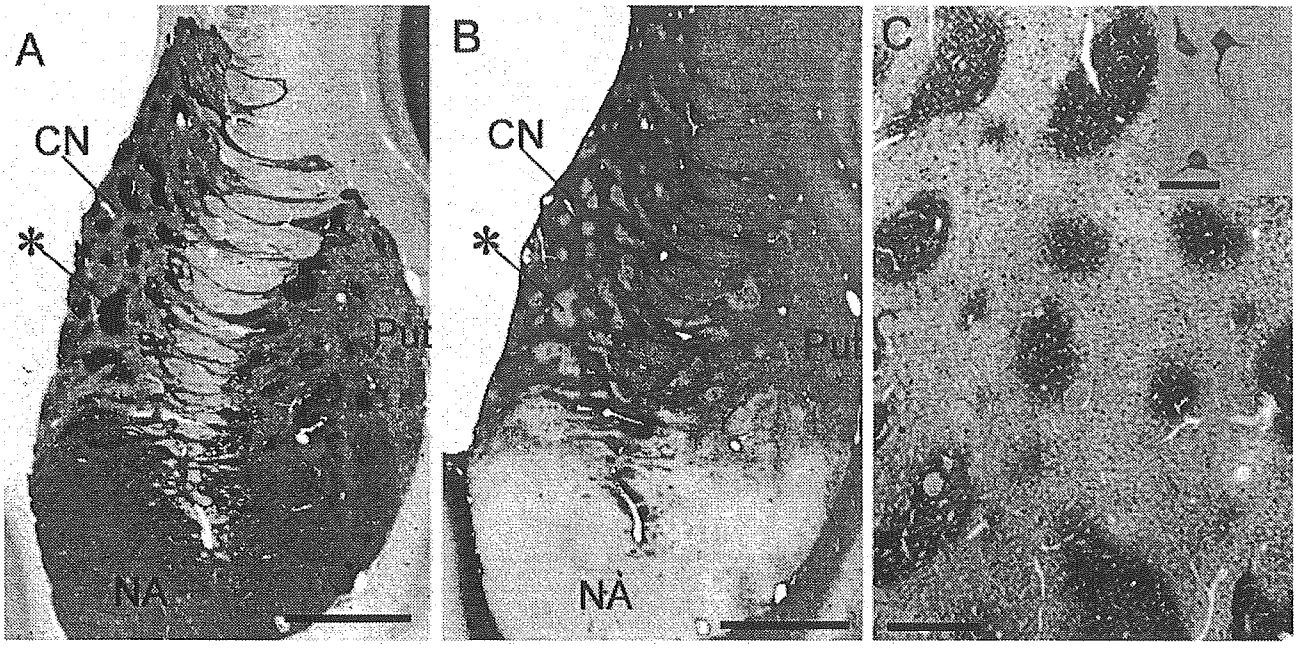

Fig 2. Neostriatal mosaic visualized by calcineurin (CaN) and glial fibrillary acidic protein (GFAP) immunostaining in X-linked recessive dystonia parkinsonism with dystonia (XDP-D). (A, B) Serially adjacent sections stained for CaN (A) and GFAP (B). The neostriatal patches visualized by CaN staining almost perfectly correspond with those poor in GFAP labeling. Asterisks *mark examples of corresponding patches. (C) Microscopically, the CaN^+ patches are composed of numerous CaN^+ neurons and their fibers. Only a few CaN^+ neurons are scattered in the interpatch area.* (inset) *High-power image of the remaining CaN^+ neurons. Scale bar (A, B) = 5mm: Scale bar (C) = 1mm: Scale bar* (inset *in C) = 50 μm. CN = caudate nucleus; Put = putamen; NA = nucleus accumbens.*

Double-Immunohistochemical Staining

Each immunostaining procedure was identical to the method described above, using the ABC method. First, the sections were processed for ChAT-immunostaining using DAB as a chromogen. The immunostained sections were again subjected to microwave-enhanced antigen retrieval and then processed for CaN-immunostaining using tetramethylbenzidine as a chromogen.

Double-Immunofluorescence Staining

Rabbit polyclonal antibody to CaN and goat polyclonal antibody to Calb (Santa Cruz Biotechnology, Santa Cruz, CA) were used as the primary antibodies. The 3 μm sections were blocked with 3% BSA-PBS for 1 hour and then incubated overnight at room temperature in 3% BSA-PBS containing the primary antibodies. Immunoreactivity was detected with fluorescein isothiocyanate– or Texas Red–conjugated secondary antibodies. Fluorescence activity was examined under a confocal laser-scanning microscope (Fluoview; Olympus Optical, Japan) and recorded.[22] Cross-reactivity between individual immunoreagents was tested with cross-fluorescence controls.

Morphometry

To determine the percent-area occupied by the CaN^+ patches in the neostriatum of XDP patients, we used Scion Image for Windows (based on NIH image). We examined 20 randomly selected sections from five XDP patients with dystonia. To determine the cell density, we counted the numbers of CaN^+ and $ChAT^+$ cells in a 1mm × 1mm field in the neostriatum. We examined 20 fields selected randomly from five XDP patients with dystonia and seven normal con-

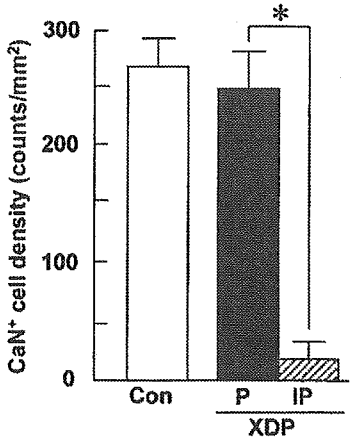

Fig 3. Cell density of CaN^+ neurons in the neostriatum. The numbers of calcineurin (CaN^+) cells/mm^2 in the neostriatum from normal controls (Con) and X-linked recessive dystonia parkinsonism (XDP) patients. Compared with controls (unfilled column), *CaN^+ neurons were well preserved in the patches (P)* (closed columns). *On the other hand, their number was severely reduced in the interpatch area (IP)* (striped column). *$^*p < 0.001$ by the two-tailed Student's t test.*

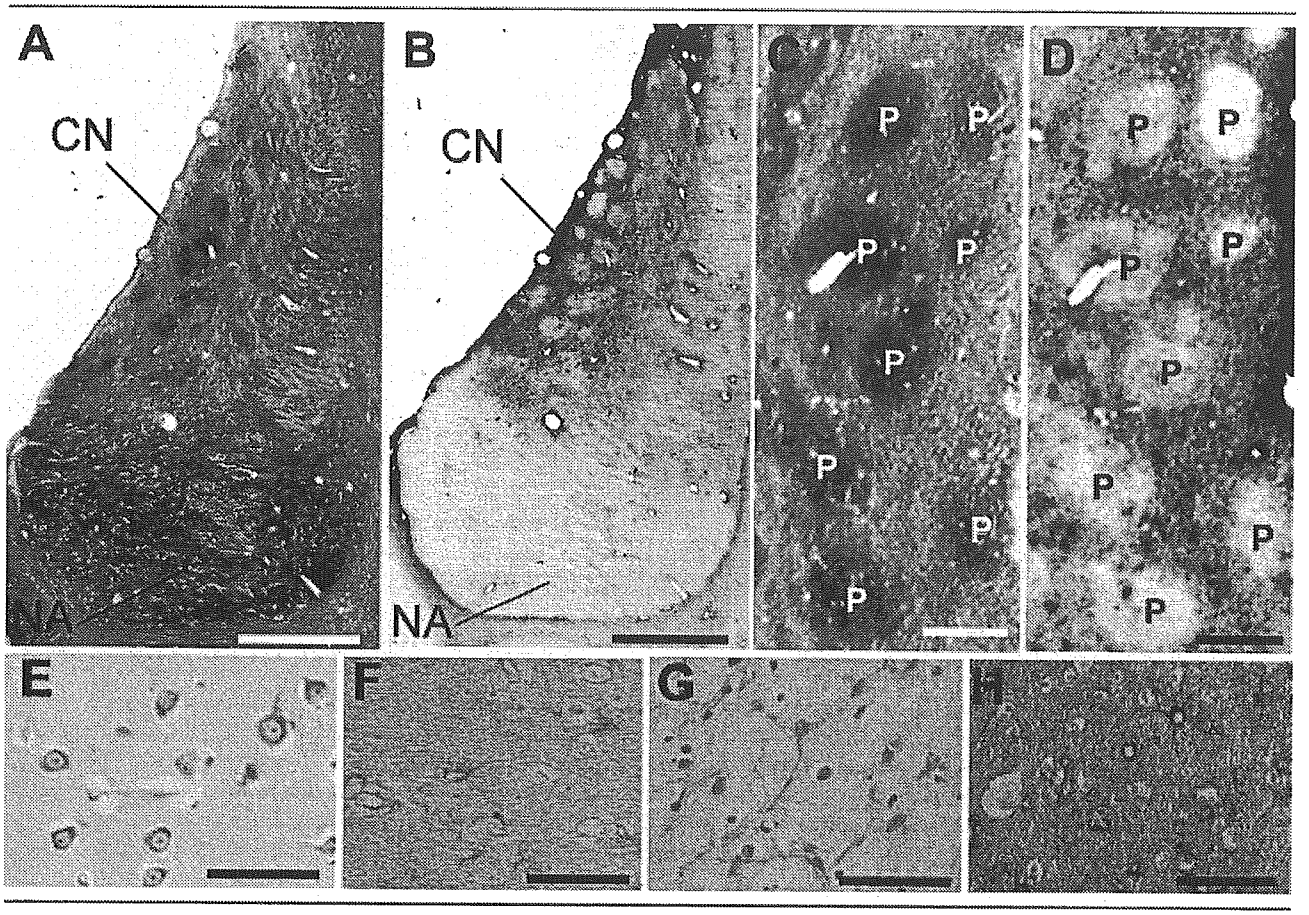

Fig 4. Mosaic appearance of neostriatal lesion visualized by Nissl and glial fibrillary acidic protein (GFAP) stains in X-linked recessive dystonia parkinsonism with dystonia (XDP-D). (A, C, E, G) Nissl staining. (B, D, F, H) GFAP staining. Low-power microscopic images of serially adjacent sections showing that the distributional patterns of Nissl (A, C) and GFAP staining (B, D) are complementary. All the patches (indicated by P*) visualized by Nissl staining are poor in GFAP staining (C, D). Under a high-power microscope, the patches appear to be normal striatal tissues (E, F). However, the interpatch area shows severe neuronal loss and astrogliosis (G, H). CN = caudate nucleus; NA = nucleus accumbens. Scale bar (A, B) = 5mm: Scale bar (C, D) = 1mm: Scale bar (E–H) = 100 μm.*

trols. For statistical analysis, we used the two-tailed Student *t* test; *p* values of less than 0.05 were considered statistically significant.

Digital Imaging

Microscopic digital images were taken with a Nikon COOLSCOPE CS1 microscope (Nikon Co, Japan). Using the software supplied with the camera, we took images at a resolution of 2,560 × 1,920 pixels, imported them into Adobe Photoshop Elements 2.0, and processed them digitally, adjusting for brightness, contrast, and sharpness. Macroscopic digital images were obtained with an Epson ES-2200 using Epson TWAIN Pro software (Epson, Japan). Images (1,600 × 3,200 DPI) were digitally processed with Adobe Photoshop Elements 2.0.

Results

Compartmental Distribution of Striatal Lesion

We first performed an immunohistochemical study using an antibody to CaN. CaN is a neurochemical marker for striatal medium spiny neurons of both the matrix and striosomal compartments and for their axonal projections in the human basal ganglia.[17–19] The medium spiny neurons account for up to 95% of the striatal neuron population; they are the primary source of striatal efferent projections that form the fundamental basic circuits of the basal ganglia.[23] In normal controls (Fig 1A), strong CaN labeling is diffusely distributed in the striatum. However, in XDP patients with dystonia (XDP-D patients), we found that macroscopically there exist two distinct compartments in the neostriatum, that is, CaN-positive (CaN^+) patches and interpatch area poor in CaN labeling (see Fig 1B). The nucleus accumbens appeared to be normal. In the XDP patients who had parkinsonism in the advanced stage (XDP-P patients), CaN labeling was markedly diminished in the entire neostriatum and CaN^+ patches were rarely found (see Fig 1C).

In XDP-D patients, the neostriatal mosaic visualized by CaN labeling (Fig 2A) was also identified upon

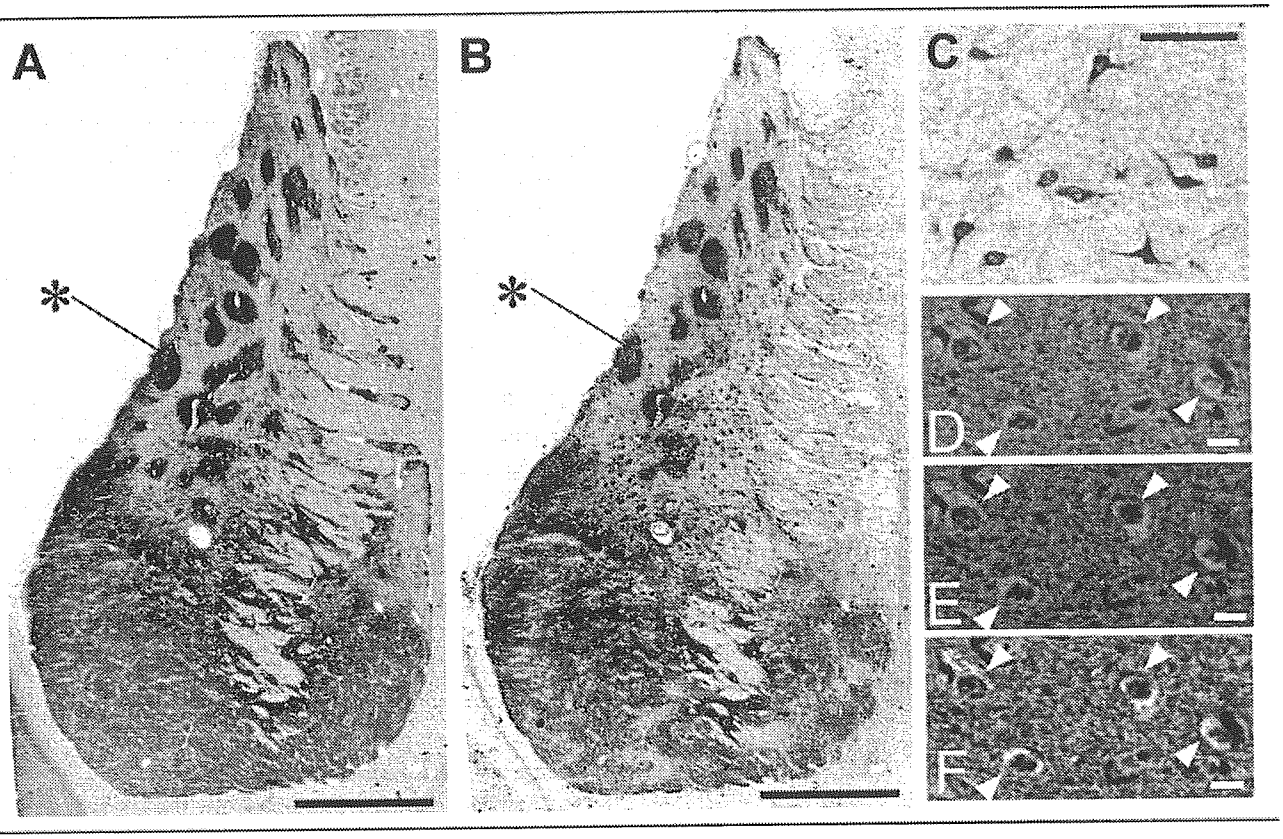

Fig 5. Correspondence of CaN^+ patches with $Calb^+$ patches in the X-linked recessive dystonia parkinsonism with dystonia (XDP-D) neostriatum. (A, B) Serially adjacent sections stained for CaN (A) and Calb (B). The neostriatal patches visualized by CaN staining almost perfectly correspond with those visualized by Calb staining with respect to their shape, size, and distribution. Asterisks *mark examples of corresponding patches. The inhomogeneous distribution of Calb labeling is normal in the nucleus accumbens. (C) High-power microscopic image of the remaining $Calb^+$ neurons. (D–F) Double-immunofluorescence staining for CaN (green) and Calb (red). CaN^+ neurons* (arrowheads *in D) are also positive for Calb* (arrowheads *in E). A merged image is shown in F. Scale bar (A, B) = 5mm: Scale bar (C) = 100 μm: Scale bar (D–F) = 20 μm.*

GFAP staining (Fig 2B). However, the distributional profiles of CaN and GFAP labeling were complementary; all CaN^+ patches were poor in GFAP staining. Microscopic observation showed that the CaN^+ patches were composed of neuron clusters and that the interpatch area contained only few neurons (see Fig 2C). Thus, the neostriatal lesion was characterized by neuronal loss and astrogliosis, and it was not diffusely but rather compartmentally distributed in a multifocal or mosaic fashion. Morphometry showed that in the caudate nucleus and putamen, CaN^+ patches occupied $36.4 \pm 4.2\%$ ($n = 20$) and $28.7 \pm 4.3\%$ ($n = 20$) of the area, respectively ($p < 0.01$). Cell-density analysis (Fig 3) disclosed that the number of CaN^+ cells/mm^2 in the neostriatum of normal controls was 270 ± 24 ($n = 20$). In XDP-D patients, it was 248 ± 32 ($n = 20$) and 24 ± 20 ($n = 20$) in the CaN^+ patches and interpatch area, respectively ($p < 0.001$). Thus, in XDP-D, neostriatal projection neurons were preserved almost normally in the CaN^+ patches; however, they were severely depleted in the interpatch area. This observation was further supported by the results we obtained with Nissl staining (Fig 4); the mosaic appearance resulted from islands (patches) of almost normal striatum sharply demarcated by gliotic area containing only a few neurons.

To determine whether the CaN^+ patches found in XDP-D originated from the striatal matrix compartment or striosomes, we used immunostaining with antibody to Calb, an excellent marker for labeling the matrix compartment.[12,24] Analysis of serially adjacent sections showed that the CaN^+ patches almost perfectly corresponded with the $Calb^+$ patches in their shape, size, and distribution (Fig 5A, B). Microscopically, $Calb^+$ patches consisted of numerous $Calb^+$ neurons and their fibers (see Fig 5C). Double-immunofluorescence staining disclosed that CaN^+ neurons represented a population that colocalized with Calb (see Fig 5D–F). These findings indicated that, in the XDP-D neostriatum, the matrix compartment was relatively spared in a mosaic pattern. However, the striosomal compartment was severely depleted because of severe neuronal loss and astrogliosis in the inter-